ACS APPLIED MATERIALS & INTERFACES

Research Article

www.acsami.org

Three-Dimensional Plasmonic Photoanodes Based on Au-Embedded TiO_2 Structures for Enhanced Visible-Light Water Splitting

Zhaoyao Zhan, Jianing An, Huanchao Zhang, Reinack Varghese Hansen, and Lianxi Zheng*

School of Mechanical and Aerospace Engineering, Nanyang Technological University, Nanyang Avenue 50, Singapore, 639798

Supporting Information

ABSTRACT: Plasmon-assisted visible light photocatalysis presents a possible solution for direct solar-to-fuel production. Here we investigate the plasmon-enhanced photocatalytic water splitting using different TiO_2/Au electrode structures. Experimental data demonstrates that the Au embedded in TiO_2 (Au-in-TiO_2) electrode greatly outperforms the Au sitting on TiO_2 (Au-on-TiO_2) electrode. Numerical simulation shows that the local electric field is very intense in the semiconductor near Au nanoparticles, which causes the enhancement of electron−hole pair generation. A 3D Au-embedded TiO_2 structure is thus proposed to further improve the light absorption and photocatalytic performance.

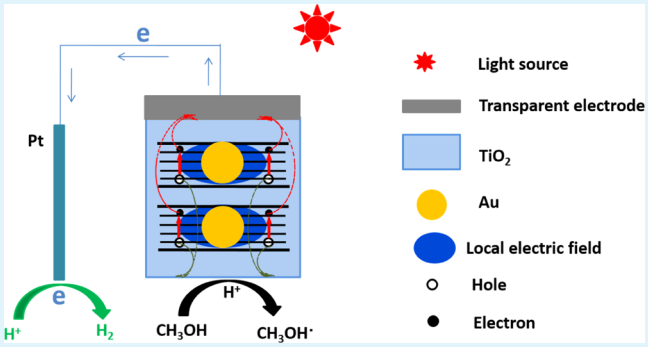

KEYWORDS: *plasmonic, photocatalytic, water splitting, local electric field, absorption*

1. INTRODUCTION

Photoelectrochemical (PEC) cells, which directly split water at the semiconductor−electrolyte interface by using solar energy, have attracted a lot of interest because of the potential for cost-effective production of hydrogen for renewable energy.[1−5] Traditional PEC electrodes utilized wide bandgap metal oxide semiconductors, such as TiO_2, ZnO, and ZrO_2, owing to their proper energy level alignments.[6] Among all these semiconductors, TiO_2 has been most widely investigated because of its low cost and good photochemical stability. Nevertheless, its large band gap requires high energy photons (larger than around 3.3 eV), which lie in ultraviolet light zone and constitute a small portion of the sun light. Various strategies have been proposed to improve the efficiency of PEC water splitting on TiO_2 electrodes. All these efforts could be categorized into several approaches, including surface modification with low bandgap semiconductors or other light absorbers,[7−16] elemental doping,[17−21] crystal structure control and so on.[22−25] While elemental doping has been employed to narrowband gap in wide gap semiconductors, so as to improve visible-light absorption,[19,21,26,27] it suffers from the inherent drawback whereby dopants act as carrier recombination centers, hampering the water splitting ability of the PEC cell. The crystal control is also a possible approach to improve efficiency of wide gap semiconductor PEC electrode by increasing the number of active sites and carrier concentrations[25] and even changing electronic structures.[28] The surface modification method is arguably, the most promising strategy because of the potential to design the light absorption and boost charge separation.[7,10,12,13,16] Photosensitization of the wide gap semiconductors with low band gap semiconductors or noble metal decoration are generally used in surface modification methods.

Recently, the use of noble metallic nanostructures has been demonstrated to be extremely effective in promoting a wide range of photocatalytic reactions.[6,14,15,29−34] The primary reason of the enhancement is attributed to the surface plasmon resonance (SPR) effect on noble metal nanostructures excited mainly by visible light illumination. Plasmon resonance phenomenon has gained considerable interest in many applications, including solar cells,[35,36] surface enhanced Raman scattering,[37−39] and photocatalysis.[14,31,32,34] Various enhancement mechanisms have been proposed, including SPR-mediated charge injection from metal to semiconductor and plasmonic heating. In the SPR-mediated charge injection mechanism, the plasmonic metal structures behave like light absorber, and charge carriers are directly injected from excited plasmonic metal structures into the adjacent semiconductor, in a manner analogous to dye sensitization.[40,41] In these systems, the photoreactions take place at the metal-semiconductor-liquid three phase boundaries (TPB). Under this condition, once excited by SPR, the electrons are moved from plasmonic metal structures to the conduction band of semiconductor and then drive the reduction reaction, such as hydrogen evolution. Another mechanism was also put forward to explain plasmonic effect in some systems where the direct charge exchanges were suppressed.[14,42] In this mechanism, SPR is able to enhance the local electric fields in the vicinity of the metal particles, and the interaction of local electric fields with the proximate semi-

Received: October 26, 2013
Accepted: January 6, 2014
Published: January 6, 2014

   dx.doi.org/10.1021/am404738a | ACS Appl. Mater. Interfaces 2014, 6, 1139−1144

conductor allows for the facile generation of electron−hole pairs in the interfacial area of the noble metal-semiconductor.[31,32,34]

Here we fabricated a new structure by embedding Au nanoparticles into the matrix of TiO_2 and observed a dramatically enhanced light absorption and photocatalytic water splitting under visible light illumination. We found that the direct charge exchange between liquid phase and Au nanoparticles was not a critical process for the visible-light induced photocatalytic water splitting on plasmonic hybrid nanostructures, which contrasts with the previously reported results.[40,41] Intriguingly, water splitting performance of Au-in-TiO_2 electrode is superior to that of Au-on-TiO_2 electrode. This observation seems to indicate that that 3D structures with multi-layer plasmonic metal structures formed by alterative depositions of Au nanoparticles and TiO_2 layers could show higher light absorption and more enhanced photocatalytic water splitting. Subsequent studies on 3D plasmonic electrodes did indeed show improved photocatalytic water splitting, which we attribute to enhanced light absorption by the 3D structure.

2. EXPERIMENTAL SECTION

2.1. Electrode Fabrication. To fabricate PEC electrodes, the TiO_2 (anatase, purity 99.99%) layer was first deposited unto fluorine-doped tin oxide(FTO) coated glass slide by a radio-frequency (RF) sputtering method, with a RF power of 100 W, Ar as carrier gas, and a stable pressure of 1.3 Pa. Then a 5 nm thick Au layer was deposited unto the surface of TiO_2 by a direct current sputtering system. The electrodes were then prepared by annealing the deposited layers at 600 °C for 1 h to improve crystallinity of TiO_2 layer and also convert gold film into a two-dimensional array of nanoparticles. The 3D Au-embedded TiO_2 electrodes were prepared by repeating the TiO_2 deposition and Au deposition process.

2.2. Characterization of Photoactivity of PEC Electrodes. The morphology of TiO_2/Au structures were observed by field-emission scanning electron microscopy (FE-SEM, JEOL JSM-7400F) with 5 KV accelerating voltage. The light absorption of the electrodes was characterized by a UV−vis spectroscopy (Shimazu UV-2400). The X-ray diffraction was collected on X-ray diffractometer with Cu K_α radiation (Rigaku D/max-B, λ = 0.15406 nm).

In photoactivity measurements, a TiO_2/Au electrode, Ag/AgCl electrode, and platinum electrode function as the working electrode, reference electrode and counter electrode respectively. The methanol (methanol% = 25%) is used as holes scavenger. The PEC electrode was irritated by a Xenon light lamp equipped with optical filters. Before the measurement, the electrolyte was first saturated by N_2 to degas electrolyte solution.

2.3. Electric Field Simulation. The simulations were carried out using the commercial finite-difference-time-domain (FDTD) software package Lumerical FDTD Solutions 8.5. All electrode models were constructed based on the structures shown in Figure 1. The geometries of the Au nanoparticles and the TiO_2 matrix were estimated according to the SEM images (Figure 2). The optical properties (i.e., complex electric permittivity) of TiO_2 were derived from the absorption spectrum of TiO_2 and that of Au were from ref 43. To avoid simulation artifacts from the meshing of the thin dielectric layer, a 1 nm air gap was used between the Au and the TiO_2 matrix. The simulation volume was 100 nm (x) by 100 nm (y) by 300 nm (z) with periodic boundaries along the x-axis and y-axis and perfectly matched layer boundaries along the z-axis. A plane wave propagating along the $-z$ direction was used as the excitation source.

3. RESULTS AND DISCUSSION

To investigate the charge transfer behavior and also enhanced light absorption in TiO_2/Au based PEC electrodes, three electrode structures were designed by alternatively depositing

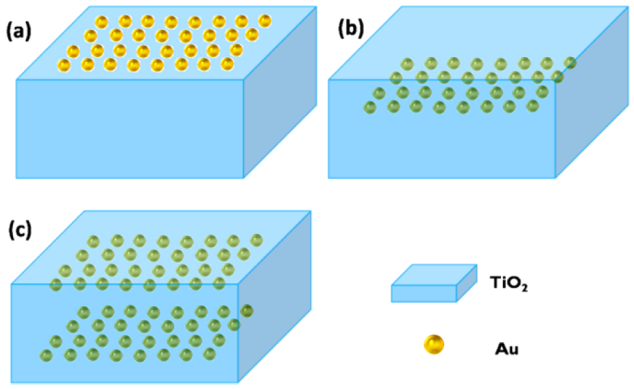

Figure 1. Schematic illustrations of (a) Au-on-TiO_2 electrode (Au particles sitting on the surface of TiO_2 layer), (b) Au-in-TiO_2 electrode (Au particles embedded in TiO_2 matrix), and (c) 3D Au-embedded TiO_2 electrode (two layers of Au particles embedded in TiO_2 matrix). The total thickness of TiO_2 is 300 nm for all three electrodes.

TiO_2 and gold layers. The Figure 1a shows the Au-on-TiO_2 electrode, which was prepared by depositing 300 nm thick TiO_2 and 5 nm thick gold layer onto a FTO substrate and then converting the Au film into fine nanoparticles by thermal annealing at 600 °C for 1 h; Figure 1b shows the Au-in-TiO_2 electrode, which was prepared using the similar process, but the thickness of TiO_2 under Au layer is 150 nm and another 150 nm thick TiO_2 layer was deposited after thermal annealing to cover the Au nanoparticles; the 3D Au-embedded TiO_2 electrode was fabricated by repeating the above processes, with the thickness of each TiO_2 layer as 100 nm, and the total TiO_2 thickness as 300 nm, as seen in Figure 1c.

After one hour thermal annealing at 600 °C, the gold film in Au-on-TiO_2 structure could be converted into fine nanoparticles with a diameter ranging from 20 to 50 nm, as shown in Figure 2a. The film-to-particles evolution was widely attributed to a thermally activated Ostwald ripening process, in which larger particles will consume smaller particles by atom migration and become larger; the driving force of this process is to reduce surface energy.[44] It is also observed that the TiO_2 film could drastically constrain the size evolution compared with FTO or glass substrate (Supporting Information Figure S1). To fabricate the Au-in-TiO_2 electrode, another layer of 150 nm thick TiO_2 was sputtered to the Au-on-TiO_2 electrode. As shown in the Figure 2b, the TiO_2 almost fully covered the Au nanoparticle layer, which could not be detected even by EDX spectroscopy. Another run of thermal annealing was applied to improve the crystallinity of the top TiO_2 layer. To observe the size evolution of Au particle embedded in TiO_2, a control sample with a very thin top TiO_2 layer was checked by SEM (Supporting Information Figure S1c). It is also observed that the gold nanoparticles didn't change their morphology and size during the later thermal annealing. The 3D Au-embedded TiO_2 electrode was fabricated by alternatively stacking TiO_2 layers and Au nanoparticle layers to form a photonic crystal-analogous structure. The cross-section image of such a structure is shown in Figure 2c: the thickness of each TiO_2 layer is about 100 nm with 2 layers of Au nanoparticles embedded in the matrix. The XRD pattern in Figure 2d further confirms the compositions of the structure, with the TiO_2 matrix being readily indexed as anatase phased TiO_2 (PDF 71-1166).

The light absorption performance of three structures was evaluated by UV-vis spectroscopy. We found a synergic effect in

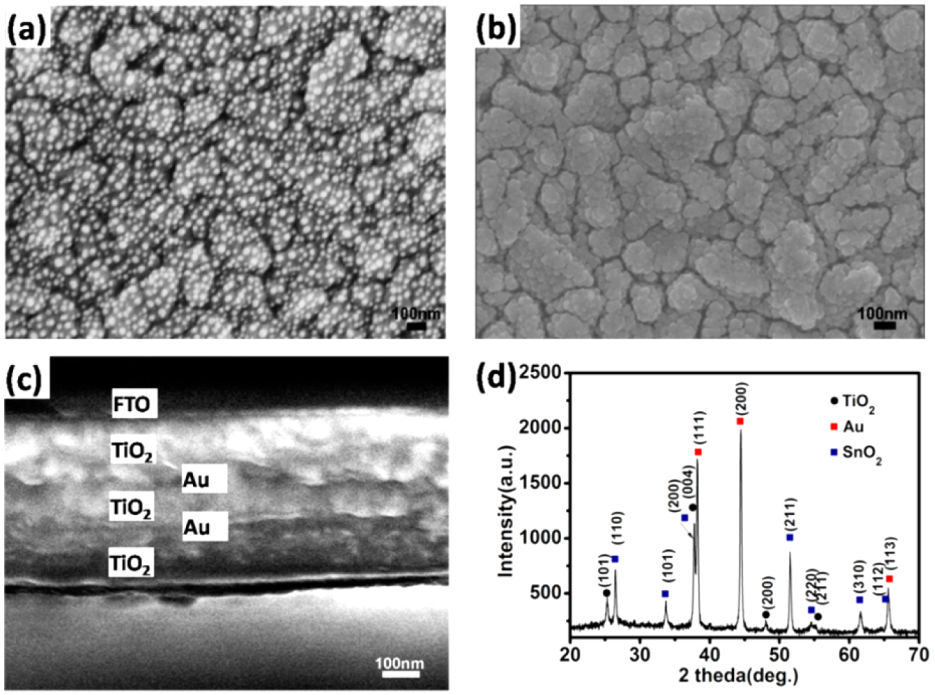

Figure 2. (a) Top view SEM image of Au-on-TiO_2 electrode. (b) Top view SEM image of Au-on-TiO_2 electrode. (c) SEM cross-section of 3D Au-embedded TiO_2 electrode (the FTO conductive substrate is on the top of the image; the section under the gap is the sample holder). (d) XRD pattern of 3D Au-embedded TiO_2 electrode.

the TiO_2/Au nanostructures. As shown in Figure 3, the TiO_2 film alone does not show a significant absorption in the range between 400 and 800 nm, and the threshold of absorption is around 400 nm. After deposition of Au onto the TiO_2 surface, the Au-on-TiO_2 electrode shows a much enhanced absorption in the visible light range, with the absorption peak shifting to long wavelength (~625 nm). We attribute this phenomenon to the synergic effect of the dielectric interaction between plasmonic metal and the local dielectric environment (semiconductor layer). The absorption could be further improved by surrounding the Au nanoparticles within the semiconductor, as shown by the absorption of Au-in-TiO_2 electrode. Once the TiO_2 covers the gold particles, the magnitude of the absorbance is further improved compared with the Au-on-TiO_2 electrode, regardless of the same total thickness of the TiO_2 matrix. This absorption improvement is even more significant in 3D Au-embedded TiO_2 electrode. This is because that a larger volume of TiO_2 are contributing to the photon absorption when more plasmonic nanoparticles are included in TiO_2 matrix. The enhanced light absorption of the 3D Au-embedded TiO_2 electrode is expected to result in enhanced photocatalytic water splitting performance.

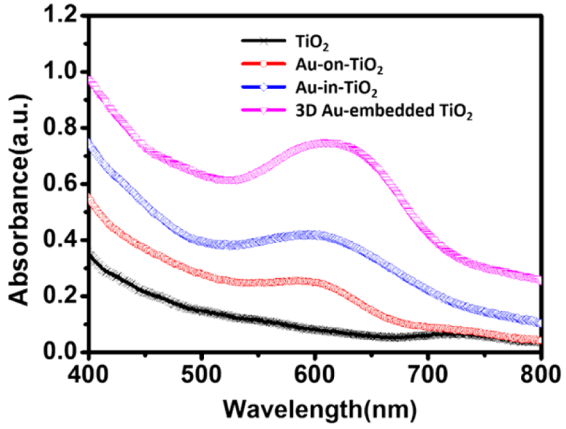

Figure 3. UV−vis absorption of TiO_2, Au-on-TiO_2, Au-in-TiO_2, and 3D Au-embedded TiO_2 electrodes.

The photoactivity of these electrodes was evaluated in a three-electrode configured PEC cell. The current−potential (I−V) curves in Figure 4 show their responses to the visible-light irradiation (wavelength >420 nm). As shown in Figure 4a, the current increases drastically once the Au-on-TiO_2 electrode exposes to the visible light, which is indicative of increase in PEC water splitting efficiency, because the current is the a direct result of water splitting on the surface of electrode. The current−time (I−t) curve of the Au-on-TiO_2 electrode shown in Figure 4b shows that current jumps to around 0.35 $\mu A/cm^{-2}$ from a negligible dark current in a very short transit time once the light irradiation is on. To evaluate the performance of the Au-in-TiO_2 electrode, the same measurement was conducted under the same conditions. The I−V characteristic of the electrode is shown in Figure 4c. Under visible light illumination, the photocurrent is again much enhanced compared with the dark current. The I−t curve of the Au-in-TiO_2 electrode shown in Figure 4d, we found the photocurrent increases to 1.1 $\mu A/cm^{-2}$ from the negligible dark current. The 3D Au-embedded TiO_2 electrode shows a more prominent performance. As shown in Figure 4e and f, under visible light illumination, the photocurrent is further enhanced. The photocurrent jumps to 1.8 $\mu A/cm^{-2}$ from the negligible dark current. The interesting observation is that the photocurrent generation increases 3 times in Au-in-TiO_2 electrode and 5 times in 3D Au-embedded TiO_2 electrode compared with that of the Au-on-TiO_2 electrode; even they have the same total thickness of TiO_2. This improvement could qualitatively agree with the light absorption results shown in Figure 3. Thus we

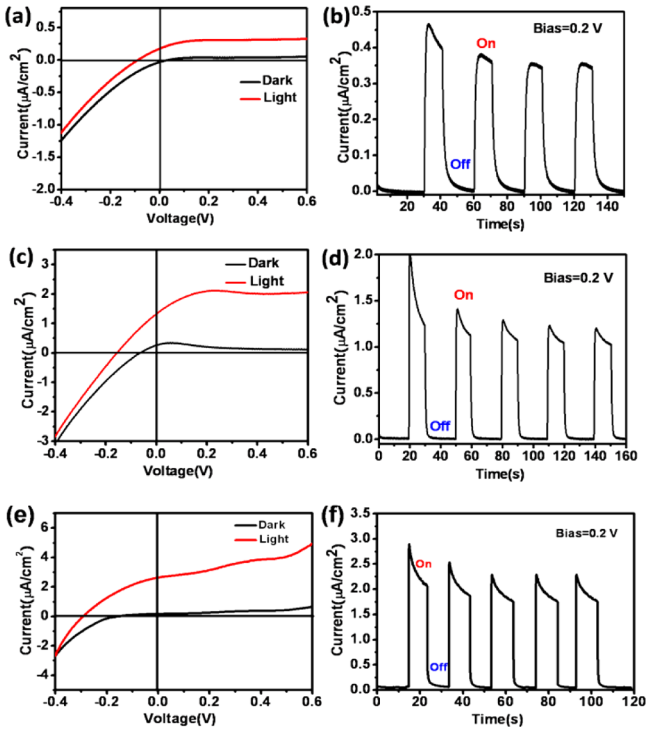

Figure 4. PEC performance of TiO_2/Au PEC electrodes irradiated by visible light (wavelength $\lambda > 420$ nm). (a) Current−potential curve of Au-on-TiO_2 electrode with visible light irradiation on and off. (b) Current−time curve of Au-on-TiO_2 electrode with visible light irradiation on and off at a bias of 0.2 V. (c) Current−potential curve of Au-in-TiO_2 electrode with visible light irradiation on and off. (d) Current−time curve of Au-in-TiO_2 electrode with visible light irradiation on and off at a bias of 0.2 V. (e) Current−potential curve of 3D Au-embedded TiO_2 electrode with visible light irradiation on and off. (f) Current−time curve of 3D Au-embedded TiO_2 electrode with visible light irradiation on and off at a bias of 0.2 V.

can attribute the enhancement in photocatalytic water splitting to the improved light absorption in the Au-in-TiO_2 and 3D Au-embedded TiO_2 electrodes.

To clarify the mechanism of this plasmonic effect on photoctatlytic performance of TiO_2/Au electrodes, FDTD code was used to simulate the electric field distribution in TiO_2/Au electrodes. The electric field simulation results are shown in Figure 5, we can observe that the electric field is converged in the proximate semiconductor area with a thickness less than 20 nm surrounding the Au nanoparticles. For Au-on-TiO_2 electrode, as shown in Figure 5a, it is obvious that the electric field surrounds the metal nanoparticles, the most intense electric field is at the contact area between plasmonic metal nanoparticle and the semiconductor, and has a magnitude of 7, which means that the photon absorption rate is enhanced by 49 times in this area (absorption is proportional to square of electric field). But please be noted that only the electric field at this limited contacting area was utilized to generate electron-hole pairs. However, for Au-in-TiO_2 electrode in Figure 5b, all electric field is confined in the surrounding semiconductor matrix, and the electric field in all space that surrounds the plasmonic nanoparticles are much higher than the value of Au-on-TiO_2 electrode. In 3D Au-embedded TiO_2 electrode, both the top and bottom Au plasmonic layers contribute to photon absorption, as shown in Figure 5c. The most intense spots around the top Au plasmonic layer reach a magnitude of 9; the

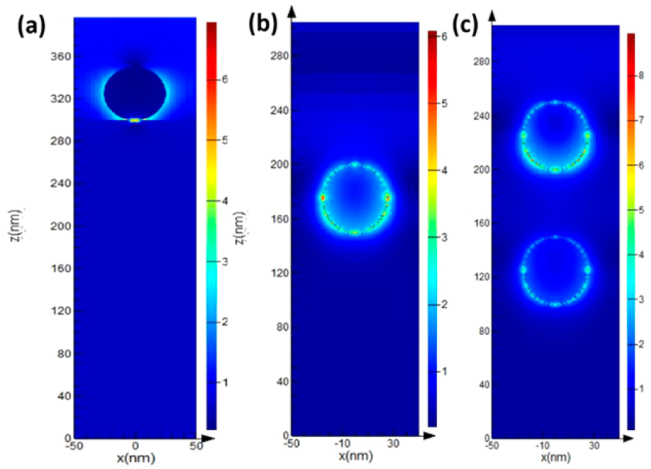

Figure 5. Electric field distribution in TiO_2/Au electrodes, in which the size of Au nanoparticles is 50 nm with center-to-center interspace of 100 nm, total thickness of TiO_2 is 300 nm, the colormap on the right side of each figure represents the electric field enhancement factor. (a) Au-on-TiO_2, (b) Au-in-TiO_2, and (c) 3D Au-embedded TiO_2 electrode with two Au layers embedded in TiO_2.

bottom layer absorbs slightly less than the up layers, but it still contributes much to the absorption of the whole electrode. These calculations agree well with the absorption spectra and photoresponse curves.

Various mechanisms have been proposed to explain the plasmon enhanced photocatalysis in the past decades.[15,31−34] The direct charge injection mechanism was found to function in composites where plasmonic nanoparticles are in direct contact with semiconductor. In these systems, the photo-reaction centers are at metal/semiconductor/liquid TPB, and they spread away from the TPB along the semiconductor/liquid interface. In our experiment, we covered the plasmonic nanoparticles with the semiconductor matrix, thus a direct TPB may not formed along the liquid/semiconductor interface. In addition, we should also be noted that the semiconductor layer covering on plasmonic nanoparticles would prevent or mitigate the direct charge exchange for photoreaction. However, we observed the opposite result that is: the Au-in-TiO_2 electrode outperformed the Au-on-TiO_2 electrode by a factor of 3. Thus here, we proposed that, the near-field electromagnetic mechanism might dominate the plasmon induced enhancement in photocatalytic activity observed in our experiments, though we could not absolutely rule out the possibility of direct charge injection in some parts (because of TPB formed at imperfect sides in TiO_2 thin films, such as voids, cracks). When the semiconductor is brought into proximity of an excited plasmonic nanostructure, it situates in the intense electric field, as the rate of electron-hole generation in a semiconductor is proportional to the square of local intensity of electric field,[16,45] thus we could observe the enhanced photocatalytic water splitting. As observed in the simulated electric field distribution (Figure 5a−c), most of electric fields are confined in proximate semiconductor around the plasmonic nanoparticles, and thus the SPR-induced electron-hole pair formation is highest in the region closet to the plamsonic nanoparticles. On the basis of above observation and analysis, a schematic mechanism was proposed in Figure 6. Once the plasmonic nanoparticle is excited by the visible light, a very strong local electric field will be formed in the proximate semiconductor matrix because of the SPR. Electron−hole pair

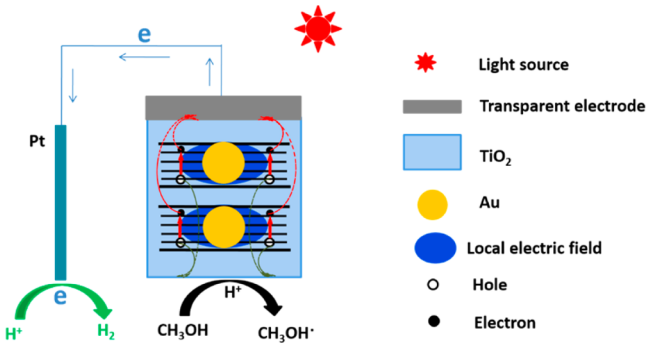

Figure 6. Proposed mechanism of plasmon-induced electron–hole pair formation in semiconductor by the local electric field in the contacting area between Au nanoparticle and semiconductor and the later photocatalytic water splitting process, in which the separated electron will transport to platinum counter electron to drive hydrogen evolution, and separated hole will transport to the semiconductor/liquid interface and be captured by the hole scavenger methanol.

could form in the strong local electric field even though the excitation energy of the visible light is lower than band gap of TiO_2. After separation, electron would transport to platinum counter electrode through the charge collecting electrode to drive the hydrogen generation, and hole will transport to the semiconductor/liquid surface and be captured by hole scavenger in liquid phase.

4. SUMMARY

In conclusion, we explore the mechanism of plasmon-enhanced photocatalytic water splitting in visible light region by exploiting different TiO_2/Au structures. Both experimental data and numerical simulation demonstrate that the enhancement in the performance of photocatalytic activity of TiO_2/Au PEC electrode could be achieved by optimizing the electrode structure. The Au-in-TiO_2 electrode greatly outperformed the Au-on-TiO_2 electrode, and 3D Au-embedded TiO_2 electrode could further improve the photocatalytic performance because of the enhanced light absorption. The intense local electric field in the proximate semiconductor surrounding plamsonic nanoparticles helps to generate electron–hole pairs, even though the excitation energy of the visible light is lower than the band gap of TiO_2. After separation, electron would transport to platinum counter electrode to drive the hydrogen evolution reaction, and hole will transport to the semiconductor/liquid surface and be captured by hole scavenger in liquid phase. The 3D plasmonic metal/semiconductor structures will provide a new pathway towards making full use of light photons for energy conversion.

■ ASSOCIATED CONTENT

Ⓢ Supporting Information

Additional SEM images of Au nanoparticles in/on different structures after annealed at 600 °C for 1 h. This information is available free of charge via the Internet at http://pubs.acs.org/.

■ AUTHOR INFORMATION

Corresponding Author

*E-mail: Lxzheng@ntu.edu.sg. Phone: (+65) 6790 4163.

Notes

The authors declare no competing financial interest.

■ REFERENCES

(1) Fujishima, A.; Honda, K. *Nature* **1972**, *238*, 37–38.
(2) Khan, S. U. M.; Al-Shahry, M.; Ingler, W. B. *Science* **2002**, *297*, 2243–2245.
(3) Maeda, K.; Teramura, K.; Lu, D. L.; Takata, T.; Saito, N.; Inoue, Y.; Domen, K. *Nature* **2006**, *440*, 295–295.
(4) Wolcott, A.; Smith, W. A.; Kuykendall, T. R.; Zhao, Y. P.; Zhang, J. Z. *Small* **2009**, *5*, 104–111.
(5) Zou, Z. G.; Ye, J. H.; Sayama, K.; Arakawa, H. *Nature* **2001**, *414*, 625–627.
(6) Linic, S.; Christopher, P.; Ingram, D. B. *Nat. Mater.* **2011**, *10*, 911–921.
(7) Liu, H. R.; Yang, J. H.; Zhang, Y. Y.; Chen, S. Y.; Walsh, A.; Xiang, H. J.; Gong, X. A.; Wei, S. H. *Phys. Chem. Chem. Phys.* **2013**, *15*, 1778–1781.
(8) Hwang, Y. J.; Boukai, A.; Yang, P. D. *Nano Lett.* **2009**, *9*, 410–415.
(9) Lv, X. J.; Zhou, S. X.; Zhang, C.; Chang, H. X.; Chen, Y.; Fu, W. F. *J. Mater. Chem.* **2012**, *22*, 18542–18549.
(10) Xiang, Q. J.; Yu, J. G.; Jaroniec, M. *J. Am. Chem. Soc.* **2012**, *134*, 6575–6578.
(11) Allam, N. K.; Yen, C. W.; Near, R. D.; El-Sayed, M. A. *Energy Environ. Sci.* **2011**, *4*, 2909–2914.
(12) Yu, J. G.; Ran, J. R. *Energy Environ. Sci.* **2011**, *4*, 1364–1371.
(13) Zhang, X. Y.; Li, H. P.; Cui, X. L.; Lin, Y. H. *J. Mater. Chem.* **2010**, *20*, 2801–2806.
(14) Awazu, K.; Fujimaki, M.; Rockstuhl, C.; Tominaga, J.; Murakami, H.; Ohki, Y.; Yoshida, N.; Watanabe, T. *J. Am. Chem. Soc.* **2008**, *130*, 1676–1680.
(15) Zhang, Z. H.; Zhang, L. B.; Hedhili, M. N.; Zhang, H. N.; Wang, P. *Nano Lett.* **2013**, *13*, 14–20.
(16) Su, F. L.; Lu, J. W.; Tian, Y.; Ma, X. B.; Gong, J. L. *Phys. Chem. Chem. Phys.* **2013**, *15*, 12026–12032.
(17) Dholam, R.; Patel, N.; Miotello, A. *Int. J. Hydrogen Energy* **2011**, *36*, 6519–6528.
(18) Liu, G.; Yin, L. C.; Wang, J. Q.; Niu, P.; Zhen, C.; Xie, Y. P.; Cheng, H. M. *Energy Environ. Sci.* **2012**, *5*, 9603–9610.
(19) Long, R.; Dai, Y.; Meng, G.; Huang, B. B. *Phys. Chem. Chem. Phys.* **2009**, *11*, 8165–8172.
(20) Frites, M.; Khan, S. U. M. *Electrochem. Commun.* **2009**, *11*, 2257–2260.
(21) Yang, X. Y.; Wolcott, A.; Wang, G. M.; Sobo, A.; Fitzmorris, R. C.; Qian, F.; Zhang, J. Z.; Li, Y. *Nano Lett.* **2009**, *9*, 2331–2336.
(22) Awate, S. V.; Deshpande, S. S.; Rakesh, K.; Dhanasekaran, P.; Gupta, N. M. *Phys. Chem. Chem. Phys.* **2011**, *13*, 11329–11339.
(23) Deshpande, A.; Madras, G.; Gupta, N. M. *Mater. Chem. Phys.* **2011**, *126*, 546–554.
(24) Liu, G.; Yang, H. G.; Wang, X. W.; Cheng, L. N.; Lu, H. F.; Wang, L. Z.; Lu, G. Q.; Cheng, H. M. *J. Phys. Chem. C* **2009**, *113*, 21784–21788.
(25) Wang, G. M.; Wang, H. Y.; Ling, Y. C.; Tang, Y. C.; Yang, X. Y.; Fitzmorris, R. C.; Wang, C. C.; Zhang, J. Z.; Li, Y. *Nano Lett.* **2011**, *11*, 3026–3033.
(26) Xu, M.; Da, P. M.; Wu, H. Y.; Zhao, D. Y.; Zheng, G. F. *Nano Lett.* **2012**, *12*, 1503–1508.
(27) Zhan, Z. Y.; Zheng, L. X.; Pan, Y. Z.; Sun, G. Z.; Li, L. *J. Mater. Chem.* **2012**, *22*, 2589–2595.
(28) Chen, X. B.; Liu, L.; Yu, P. Y.; Mao, S. S. *Science* **2011**, *331*, 746–750.
(29) Wang, T. Y.; Liu, L.; Zhu, Z. W.; Papakonstantinou, P.; Hu, J. B.; Liu, H. Y.; Li, M. X. *Energy Environ. Sci.* **2013**, *6*, 625–633.
(30) Thimsen, E.; Le Formal, F.; Gratzel, M.; Warren, S. C. *Nano Lett.* **2011**, *11*, 35–43.
(31) Thomann, I.; Pinaud, B. A.; Chen, Z. B.; Clemens, B. M.; Jaramillo, T. F.; Brongersma, M. L. *Nano Lett.* **2011**, *11*, 3440–3446.
(32) Liu, Z. W.; Hou, W. B.; Pavaskar, P.; Aykol, M.; Cronin, S. B. *Nano Lett.* **2011**, *11*, 1111–1116.
(33) Gao, H. W.; Liu, C.; Jeong, H. E.; Yang, P. D. *ACS Nano* **2012**, *6*, 234–240.

(34) Ingram, D. B.; Linic, S. *J. Am. Chem. Soc.* **2011**, *133*, 5202−5205.
(35) Ferry, V. E.; Sweatlock, L. A.; Pacifici, D.; Atwater, H. A. *Nano Lett.* **2008**, *8*, 4391−4397.
(36) Nakayama, K.; Tanabe, K.; Atwater, H. A. *Appl. Phys. Lett.* **2008**, *93* (12), No. 121904.
(37) Dou, X.; Chung, P. Y.; Sha, H. Y.; Lin, Y. C.; Jiang, P. *Phys. Chem. Chem. Phys.* **2013**, *15*, 12680−12687.
(38) Lin, H. X.; Li, J. M.; Liu, B. J.; Liu, D. Y.; Liu, J. X.; Terfort, A.; Xie, Z. X.; Tian, Z. Q.; Ren, B. *Phys. Chem. Chem. Phys.* **2013**, *15*, 4130−4135.
(39) Mechler, M.; Kukhlevsky, S. V.; Mechler, A.; McNaughton, D. *Phys. Chem. Chem. Phys.* **2011**, *13*, 20772−20778.
(40) Tian, Y.; Tatsuma, T. *J. Am. Chem. Soc.* **2005**, *127*, 7632−7637.
(41) Kowalska, E.; Mahaney, O. O. P.; Abe, R.; Ohtani, B. *Phys. Chem. Chem. Phys.* **2010**, *12*, 2344−2355.
(42) Kumar, M. K.; Krishnamoorthy, S.; Tan, L. K.; Chiam, S. Y.; Tripathy, S.; Gao, H. *ACS Catal.* **2011**, *1*, 300−308.
(43) Johnson, P. B.; Christy, R. W. *Phys. Rev. B* **1972**, *6*, 4370−4379.
(44) Zhan, Z. Y.; Zhang, Y. N.; Sun, G. Z.; Zheng, L. X.; Liao, K. *Appl. Surf. Sci.* **2011**, *257*, 7704−7708.
(45) Anger, P.; Bharadwaj, P.; Novotny, L. *Phys. Rev. Lett.* **2006**, *96*, No. 113002.